ACS APPLIED MATERIALS & INTERFACES

RESEARCH ARTICLE

www.acsami.org

Confinement of Elastomeric Block Copolymers via Forced Assembly Coextrusion

Tiffani M. Burt,[†,‡] Jong Keum,[†] Anne Hiltner,[†,‡] Eric Baer,[†,‡] and LaShanda T.J. Korley[*,†,‡]

[†]Department of Macromolecular Science and Engineering, and [‡]Center for Layered Polymeric Systems, Case Western Reserve University, Cleveland, Ohio 44106-7202, United States

Supporting Information

ABSTRACT: Forced assembly processing provides a unique opportunity to examine the effects of confinement on block copolymers (BCPs) via conventional melt processing techniques. The microlayering process was utilized to produce novel materials with enhanced mechanical properties through selective manipulation of layer thickness. Multilayer films consisting of an elastomeric, symmetric block copolymer confined between rigid polystyrene (PS) layers were produced with layer thicknesses ranging from 100 to 600 nm. Deformation studies of the confined BCP showed an increase in ductility as the layer thickness decreased to 190 nm due to a shift in the mode of deformation from crazing to shear yielding. Postextrusion annealing was performed on the multilayer films to investigate the impact of a highly ordered morphology on the mechanical properties. The annealed multilayer films exhibited increased toughness with decreasing layer thickness and resulted in homogeneous deformation compared to the as-extruded films. Multilayer coextrusion proved to be an advantageous method for producing continuous films with tunable mechanical response.

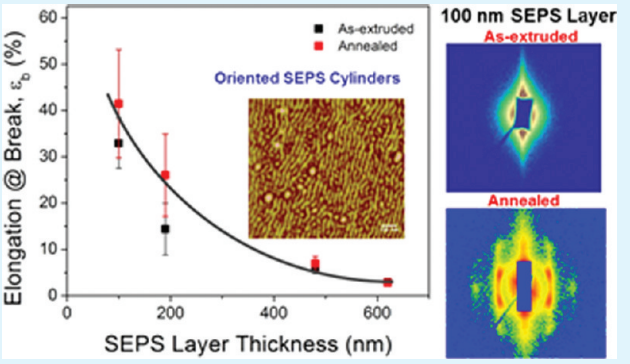

KEYWORDS: thin films, confinement, block copolymers, mechanical properties, multilayer coextrusion, elastomers

INTRODUCTION

Block copolymers (BCPs) are highly tunable materials through variations in block chemistry, molecular weight, chain architecture, and volume composition and can self-assemble into a variety of ordered microstructures, such as spherical, cylindrical, lamellar, or gyroid morpohologies, on the nanoscale.[1] Microphase separation within these novel materials can be attributed to a thermodynamically driven process that balances entropic expansion and enthalpic repulsion of the individual blocks that are attached through covalent bonds.[2−5] Details of the roles of degree of polymerization, N, and the Flory−Huggin's interaction parameter, χ, on the morphology of BCPs at various segregation limits have been published collectively in a number of reviews and book chapters.[6,7]

Confinement of polymeric systems on the nanometer scale has been the subject of many research platforms and has revealed that, under constraint, properties, such as crystallization, physical aging, permittivity, and glass transition, deviate from bulk material characteristics.[8] The bulk phase separation of BCPs has been manipulated by the constraint of confinement, which alters the block copolymer domain spacing and the microphase separation processes leading to metastable morphologies. Extensive research has been conducted in various confining geometries, such as thin films,[9−21] cylindrical pores,[22,23] or nanofibers.[24] For example, experimental and theoretical analysis of thin film geometries have revealed that the equilibrium morphology of BCPs is altered with decreasing film thickness. Cylindrical ABA block copolymers have been shown to change morphological orientation or undergo surface reconstructions as layer thickness decreases, resulting in microstructures, such as a perforated lamella, lamella, and a wetting layer.[16,18]

Technological advances in conventional polymer melt processing have provided a methodology to tune physical properties, such as gas permeability,[25] mechanical toughness,[26,27] and optical response[28,29] by varying layer thickness. Forced assembly layered coextrusion is a process by which immiscible polymers are coextruded through a series of die elements termed as "multipliers", where n multipliers produces $2^{(n+1)}$ alternating layers.[30−32] The microlayering process has been used to produce new blends and composites from two or more polymeric materials by forcing the materials into an alternating layered film with varying layer thicknesses ranging from the nanoscale to microscale.[33−35] Previous work by Baer and

Received: September 22, 2011
Accepted: November 10, 2011
Published: November 29, 2011

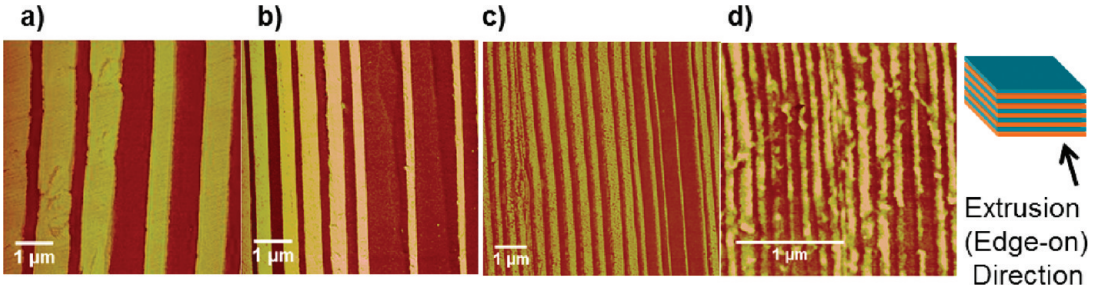

Figure 1. AFM tapping mode phase images of multilayer films of PS/SEPS with 257 layers: (a) 620 nm SEPS layer, (b) 480 nm SEPS layer, (c) 190 nm SEPS layer, (d) 100 nm SEPS layer.

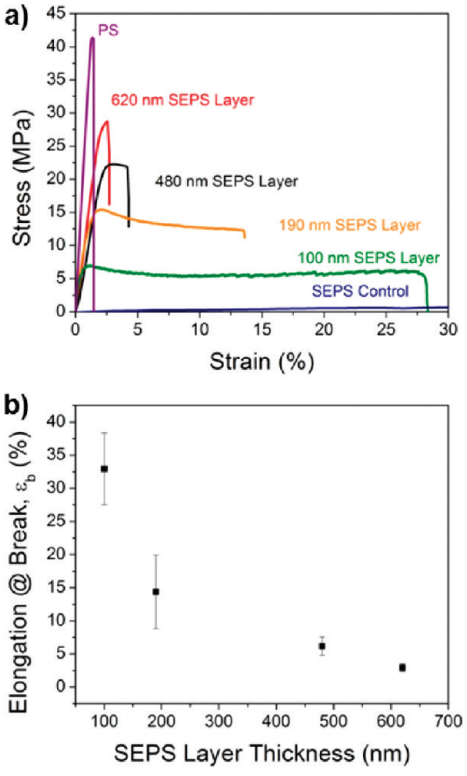

Figure 2. Mechanical response of PS/SEPS multilayer films under uniaxial deformation. (a) Stress−strain response of multilayer films. (b) Effect of layer thickness on elongation-at-break, ε_b.

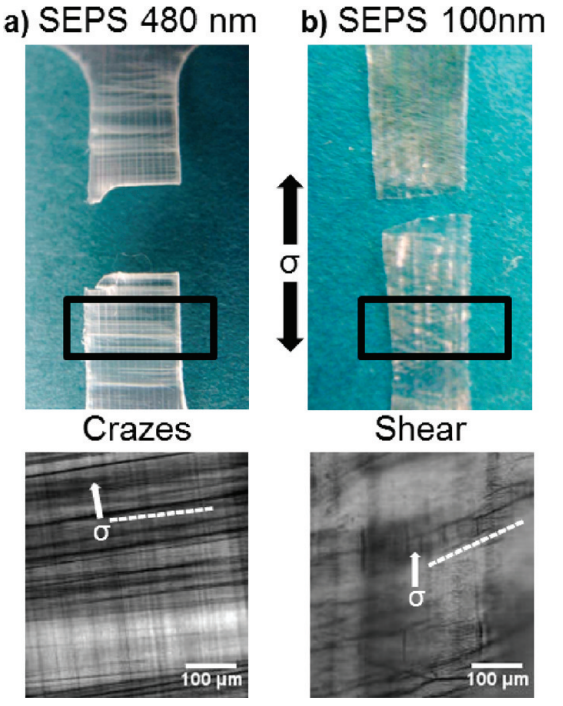

Figure 3. Optical micrographs of deformed PS/SEPS multilayer films: (a) 480 nm SEPS layer thickness, (b) 100 nm SEPS layer thickness.

Hiltner has reported increased toughness in polymer composites as a function of multilayer thickness that enables an alternate deformation mode of cooperative shear banding. The shear bands aided in the decrease of stress concentrations at the crack tip as the craze propagated across the film and led to an increase in ductility within the polymeric composite.[36−38] This layering process provides a unique platform to probe the relationship between the confinement-induced architecture of block copolymers, and mechanical function and deformation mechanisms.

In this work, we utilize microlayer coextrusion to produce multilayered films of elastomeric block copolymers confined by a glassy polymer to elucidate the deformation mechanics of multilayers as a function of layer thickness. It is our goal to understand how altering the morphology through confinement and processing of BCPs via coextrusion will impact mechanical response. With this approach, the mechanical behavior of multicomponent polymeric systems can be tuned using a commercially viable and versatile processing technique via alteration of layer thickness.

EXPERIMENTAL SECTION

Materials. Polystyrene (PS) was donated by the Dow Chemical Company, STYRON 685D (PS, Number average molecular weight, (M_n) = 128 kg/mol and dispersity ($\overline{DP}$) = 1.60). Polystyrene-*block*-polyethylene/polypropylene-*block*-polystyrene triblock copolymer (SEPS), commercially known as Kraton G1730 (M_n= 94.8 kg/mol, ($\overline{DP}$) = 1.10, styrene content ∼21% by volume), was obtained from Kraton Polymers, Inc. Molecular weights were obtained by gel permeation chromatography (GPC) on a Viscotek instrument calibrated by PS standards with toluene as an eluent at a flow rate of 1 mL/min.

Co-extruded Samples. Processing temperatures of the PS and SEPS were determined as a function of viscosity using a melt flow indexer (Galaxy I Model D7054, Kayeness Inc.) at a low shear rate,

Table 1. Mechanical Properties of As-Extruded PS/SEPS films via Uniaxial Tensile Testing

	257 layers; 50/50 (v/v)					
	620 nm	480 nm	190 nm	100 nm	SEPS control as-extruded	PS control as-extruded
elastic modulus (MPa)	852.4 ± 120	771.9 ± 382	754.2 ± 279	279.7 ± 197	1.23 ± 0.021	3510 ± 562
elongation-at-break ε_b (%)	2.94 ± 0.60	6.04 ± 1.39	14.15 ± 3.92	30.36 ± 7.48	489.7 ± 28.03	1.87 ± 0.13
ultimate tensile strength (MPa)	26.69 ± 2.09	24.50 ± 2.16	28.16 ± 3.90	4.98 ± 2.68	7.14 ± 0.19	40.45 ± 6.85
toughness (MJ/m^3)	0.11 ± 0.03	0.25 ± 0.08	0.62 ± 0.29	1.65 ± 0.54	17.63 ± 0.80	0.35 ± 0.06

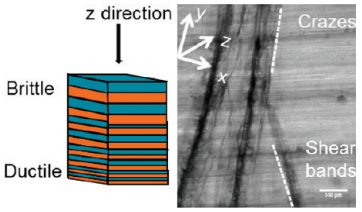

Figure 4. Confocal microscopy image of a 10× gradient multilayer film of PS/SEPS detailing crazes and shear bands in deformed multilayer films.

10 s^{-1}, to simulate flow conditions during the coextrusion process. The PS and SEPS controls were dried under vacuum for 24 h prior to microlayering to ensure minimal water uptake and coextrusion was performed at, 250 °C and 240 °C, respectively, to ensure a viscosity match in the feedblock (see Figure S1 in the Supporting Information). A 257 multilayer system was extruded with a PS layer on both sides of the films to ensure that the SEPS layers did not adhere to the chill roll. The total film thickness was varied between 25 to 250 μm at a constant volume composition of 50/50, providing equal layer thicknesses of PS and SEPS. Additionally, control samples of PS and SEPS were extruded under the same conditions.

Annealed Samples. The multilayer films and controls were annealed for 4 days under vacuum to allow sufficient time for chain mobility within the confined layers. The annealing temperature was 90 °C, which was below the glass transition temperature (T_g = 105 °C) of the PS confining layer, maintaining layer integrity.

Morphological Analysis. The layer uniformity and BCP morphology within the multilayer films were studied by atomic force microscopy (AFM). The samples were embedded in a low viscosity Spurr's resin and placed under vacuum for 7 h at 70 °C to cure the epoxy prior to cryosectioning on a Leica Ultramicrotome, UC6. The samples were cryotomed perpendicular to the edge of the film to analyze the edge-on view at a cutting temperature of −70 °C with a glass knife temperature of −60 °C. The films were analyzed under ambient conditions on a Vecco AFM in tapping mode. The tips were silicon with an oscillating frequency of 150 kHz and stiffness of 5 N/m. Tapping mode/noncontact tips were used with a tip radius of <10 nm to enable imaging of small scale features in soft materials. Both height and phase images were collected of the microlayered films perpendicular to the layer orientation and SEPS controls. In preparation for transmission electron microscopy (TEM), samples were cryomicrotomed at −100 °C with a Diatome cryodiamond knife and stained for 5 min with a 1% by weight solution of ruthenium tetroxide, RuO_4. A field-emission gun, energy-filtering TEM (Zeiss Libera 200FE) operating at 200 kV was utilized.

Small-angle X-ray scattering (SAXS) measurements were conducted using a Rigaku S-MAX 3000 SAXS system. Cu Kα X-rays from a MicroMax-002+ sealed tube source (λ = 0.154 nm) were collimated through three pinhole slits to yield a final spot size of 0.7 mm at the sample position. Multilayer films were mounted in a vacuum chamber and aligned in the extrusion direction (ED) and the transverse direction (TD) being offset ∼3° with respect to the X-ray beam to avoid total reflection, and the normal direction (ND) parallel to the X-ray beam. Two-dimensional (2D) SAXS data were collected using a Rigaku multiwire area detector with a circular active area of 133 mm and a spatial resolution of 1024 × 1024 pixels. The sample-to-detector distance and the scattering vector, q, were calibrated using a silver behenate (AgBe) standard with a characteristic (001) peak position at q = 1.076 nm^{-1}. The calculated sample-to-detector distance was 1.5 m. Typical exposure times for ED and TD SAXS patterns were 1 h, whereas ND SAXS patterns were collected for 3 h because of low scattering intensity from the SEPS.

Additional SAXS measurements were conducted at the National Synchrotron Light Source (NSLS) in the Brookhaven National Laboratory (BNL), USA on beamline X27C. The wavelength used was 0.1371 nm and the sample-to-detector distance was calculated at 1.8 m. Multilayer films were mounted in the same alignment as previously stated with acquisition times from 30 to 60 s. The two-dimensional (2D) SAXS patterns were recorded using a MarCCD X-ray detector. The diffraction angle was calibrated using a silver behenate (AgBe) standard with a characteristic (001) peak position at q = 1.076 nm^{-1}. All X-ray images were processed using software named "POLAR" (Stonybrook Technology and Applied Research, Inc.).

Uniaxial Mechanical Analysis. Uniaxial tensile deformation was performed on an Instron mechanical testing instrument at room temperature with a 1 kN load cell. The samples were cut from a steel die according to ASTM D638 with a minimum of five samples per layer thickness. The samples were placed between Mylar sheets during the cutting process to relieve stress concentrations at the edges and then smoothed with a polishing cloth to remove any defects accrued in the cutting process. The PS/SEPS multilayer films were elongated at room temperature under a constant strain rate of 10% strain per minute.

Deformation Zone Analysis. Multilayer films surfaces were imaged to examine the mode of deformation as a function of layer thickness. The films were manually stretched to 2% strain on a hand stretcher to obtain significant crazing prior to failure. Confocal microscopy images were obtained in transmittance mode on an Olympus FV 1000 in an upright configuration to analyze the multilayer films in the z-direction or through the film thickness. The microlayered film surfaces were analyzed directly by optical microscopy using an Olympus BH-2 in reflectance mode at a magnification of 120×.

RESULTS AND DISCUSSION

Multilayer coextrusion was utilized to produce films (257 layers; 50/50 volume composition) of SEPS confined against PS, where the individual SEPS layer thickness varied from 100 to 620 nm as revealed by AFM (Figure 1). Layer thicknesses varied approximately ±12% of the nominal value due to the difference in elasticity of the two polymers; improvement in the coextrusion of elastomeric materials is currently underway. This range of layer thickness was designed to provide a

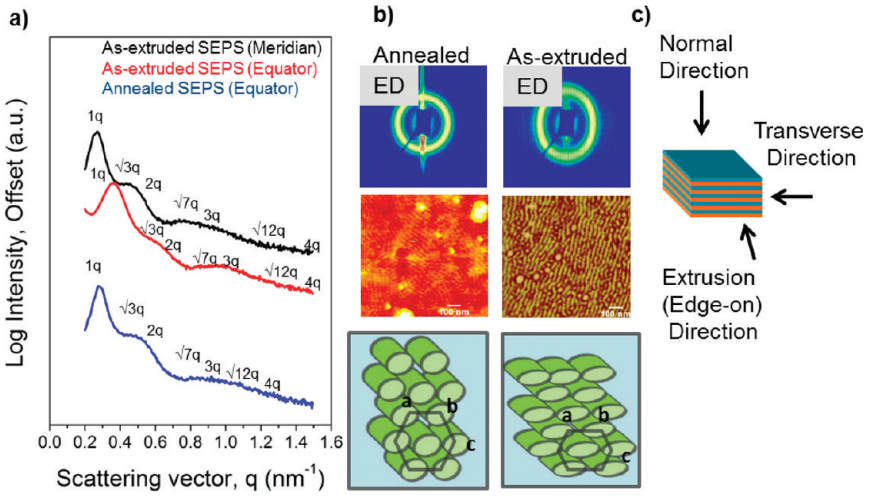

Figure 5. SAXS analysis of SEPS controls. (a) 1D scattering profiles. (b) 2D scattering patterns with accompanying AFM images of the as-extruded and annealed samples. (c) Schematic of beamline orientation to the films.

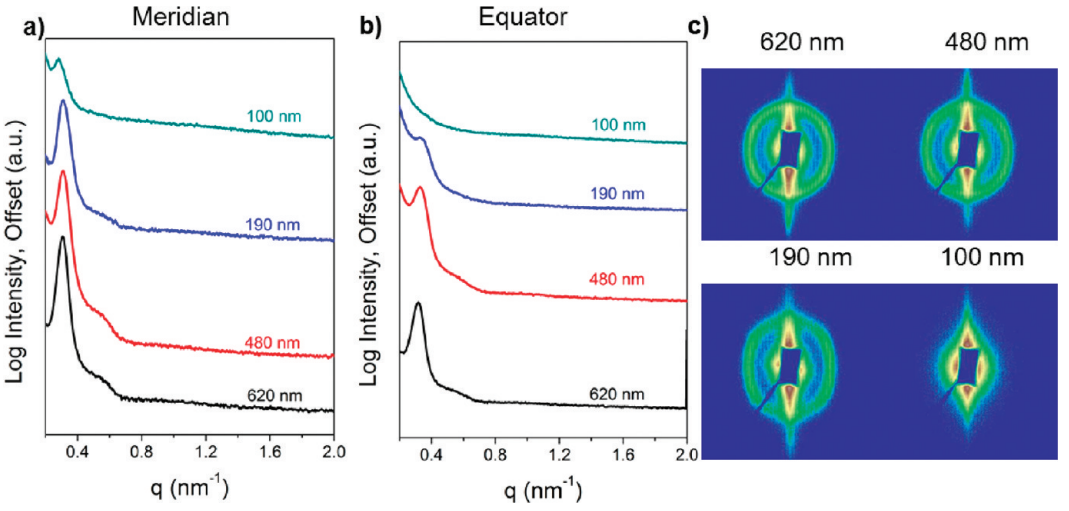

Figure 6. 1D scattering profiles of the edge-on orientation of multilayer films. (a) Meridional scan. (b) Equatorial scan. (c) 2D SAXS plots of the as-extruded multilayer films.

systematic study of the role of confinement via forced assembly on the mechanical behavior of PS/SEPS multilayered films. The mechanical response of the multilayer films was analyzed under uniaxial tension. Non-homogeneous deformation was observed during elongation of the as-extruded multilayer films. At very low strains, the PS failed in a brittle manner, while the elastomeric BCP remained intact and absorbed the residual stress until ultimate failure. As the layer thickness decreased, a shift in deformation mode resulted in a brittle-to-ductile transition. The elongation-at-break, ε_b, increased 10-fold from 3 to 30% for the 620 and 100 nm, respectively (Figure 2a). The thicker layer films, 480 and 620 nm, failed by brittle fracture at strains less than 5%, resulting in significant stress whitening accompanied by an opaque appearance upon deformation. As the layer thickness decreased to 190 nm, the ε_b reached higher strain values and the formation of a necking region was observed. The thinner films remained transparent under deformation, and large shear bands were visible after failure, indicating a shift to a yielding mechanism within the films (Figure 3). A critical layer thickness of 200 nm was noted, at which a change in deformation mechanism (Figure 2b) and toughness enhancement was observed (Table 1). Similar work by Michler et al. revealed a shift in deformation mechanics via a systematic investigation of bulk polymeric materials and layered polymeric materials generated utilizing blends, multilayer coextrusion, and self-assembly of symmetric block copolymers. In layer forming systems, deformation results in a combination of multiple crazes and shear bands resulting in increased extensibility, which has been termed thin layer yielding.[39−41] The shift in deformation mechanics was further investigated by examining multilayer films that were strained to failure via confocal and optical microscopy (Figure 3). Within the thicker layers (480 nm), crazes, which propagate at 90° to the applied tensile stress, and significant stress whitening were observed. In the thinner SEPS layers (100 nm), shear banding was detected, which is represented by striations that developed at 45° to the tensile force and remained transparent after deformation, and is indicative of yielding. A combinatorial assay of the deformation mechanics as a function

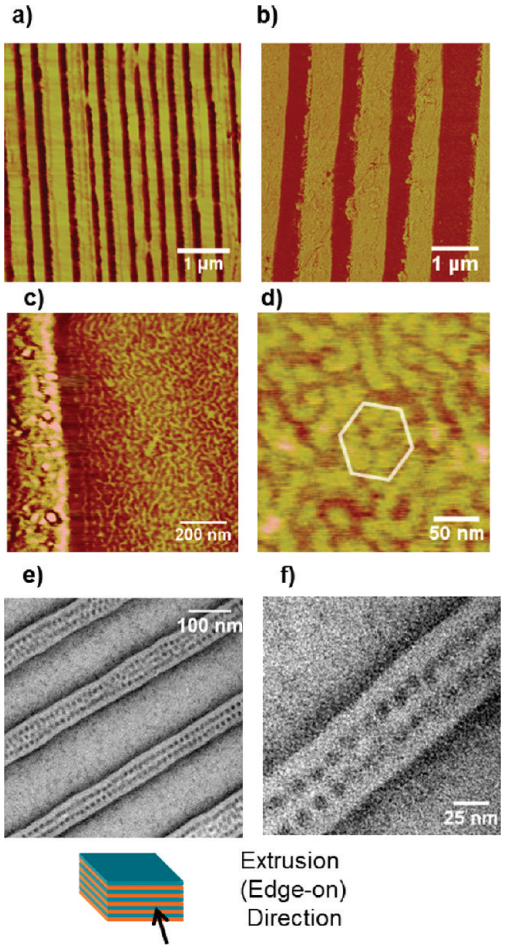

Figure 7. AFM phase micrographs of annealed multilayer films: (a) 190 nm SEPS layer; (b) 620 nm SEPS layer; (c) 620 nm SEPS layer highlighting confinement-induced assembly; (d) area of hexagonally packed cylinders within 620 nm multilayer film. (e, f) TEM micrographs of 100 nm SEPS layered sample (d, f are zoomed-in images of c and e).

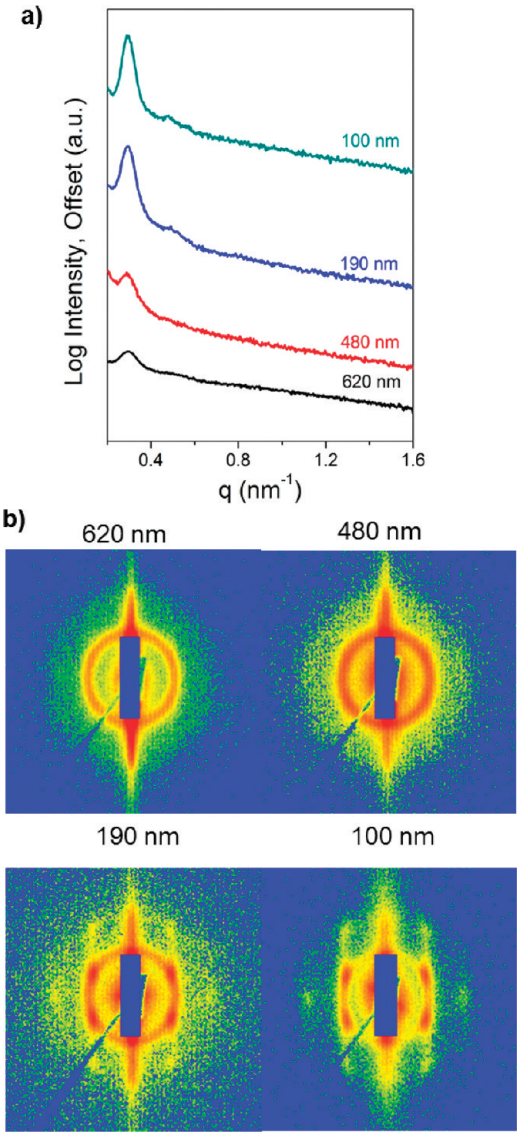

Figure 8. SAXS analysis of the annealed multilayer films with the beam aligned in the extrusion direction. (a) 1D profile of the layered films; (b) 2D scattering patterns.

of layer thickness was conducted using a gradient multilayer film prepared by forced assembly coextrusion. The 50/50 gradient films consisted of layer thicknesses with a 10× gradient (1 μm thick layers to thin layers of 100 nm) through the film thickness. These films were strained to 2% and analyzed by confocal microscopy in transmittance mode (Figure 4). In the thick, top layers of the gradient film, large crazes are observed (dark lines), which propagated across the film width (perpendicular to the applied stress). As the bottom surface of the film was approached in the z-direction, thin shear bands (light lines) were seen at 45° to the applied force. Confocal microscopy analysis confirmed a shift in the deformation mode from crazing to cooperative shear banding.[42] Because of the similar refractive indices of the two polymers, the exact layer thickness at which the two deformation mechanisms occurred could not be determined.

Critical to understanding the deformation mechanics of the multilayer films was an analysis of the BCP morphology within the layers. The as-extruded BCP was analyzed in the normal direction and exhibited ratios of q values at the peak maxima identical to $1:\sqrt{3}:\sqrt{4}:\sqrt{7}:\sqrt{9}$, which is representative of a hexagonally-packed, cylindrical array (Figure 5). The 2D scattering profile displayed arcing along the equator, indicating preferential alignment of the cylindrical rods in the extrusion direction (Figure 5). The extruded control was also analyzed edge-on and averaged over the meridian (70 to 110°) and equator (−30 to 30°), revealing a shift in the domain spacing from 23 to 19 nm, respectively. This reduced equatorial spacing was attributed to the effect of flow-induced confinement during extrusion, which distorted the cross-section of cylindrical PS domains and led to a more ellipsoidal shape[43] due to the high strains that the extruded films were subjected to from the die onto the chill roller for film thickness reduction. To confirm this hypothesis, the extruded control was annealed for 4 days at 90 °C to erase the thermal history from processing. The resulting 2D scan showed an isotropic scattering profile with an equivalent domain spacing (22 nm) when averaged along the meridian and equator.

The PS/SEPS multilayer films (257 layers; 50/50) were analyzed in the normal (ND), transverse (TD) and extrusion (ED) directions to elucidate the BCP microstructure within the layers (see Figure S4 in the Supporting Information). SAXS

patterns (ND) confirmed that the cylindrical microdomains were aligned in the extrusion direction due to flow field effects for all layer thicknesses. A narrowing of the equatorial arcs was observed with a reduction of layer thickness, as expected, suggesting a high degree of cylinder orientation within the films. The transverse direction (TD) scattering patterns also revealed more point-like meridian arcs, implying stacking of the PS cylinders through the layer thickness (see Figure S4 in the Supporting Information). As in the as-extruded control, scattering patterns were also obtained in the extrusion direction (ED) for the multilayer films (Figure 6). The degree of confinement increases with decreasing layer thickness, leading to a distortion of the hexagonal packing of the cylindrical array and a decrease in the cylindrical diameter. The scattering intensity was very diffuse in the 100 nm multilayer film, hindering detection of the BCP ordering because of minimal sampling thickness. The PS cylinders were unconfined in the x-direction (width of layer), leading to an ellipsoidal, tubular geometry in the 190 nm layers. The PS/SEPS multilayer films were analyzed postannealing through AFM to confirm layer uniformity and integrity of the layers postprocessing. Because of the elastic nature of the BCP, the layer thicknesses of the SEPS vary from the nominal thicknesses that were calculated as referenced previously (Figure 7). It can be seen that the BCP is highly phase-separated and in the thinner layers lying in-plane with the directional flow, whereas the thicker layers are more isotropic in nature. Because of the lack of contrast via AFM, TEM was performed on the thinnest layer sample, 100 nm, revealing a high degree of ordering through the layer thickness. Further investigation of the confined morphology of the BCP was conducted after annealing. Annealing eliminated the distortion of the cylindrical array, and the microdomains adopted a more entropically favored structure throughout the thickness of the BCP layer, resulting in an isotropic ring with equivalent scattering vectors along the equator and meridian (Figure 8). In the ED, the 1D scattering patterns showed a significant increase in the long-range ordering of the SEPS as a result of the additional constraint of confinement within the multilayer films as the layer thickness decreased to 100 nm. The layer thicknesses above 190 nm exhibited hexagonal packing of cylinders that were isotropic in nature through the thickness of the layer, as indicated in the 2D scattering patterns. As the thickness of the layer decreased, the mobility of the polymer chain was restricted and the original flow-induced alignment was maintained within the film. Below the 190 nm layer thickness, an unprecedented 6-point pattern was observed.[44] The PS cylinders were discovered to lie parallel to the layer surface and uniformly packed across the width and thickness of the BCP layer. The degree of ordering was attributed to the shear field introduced during the multilayer coextrusion and remained oriented post-thermal treatment in the thinner layers because of confinement effects similarly seen in work by Nealey et al.[45]

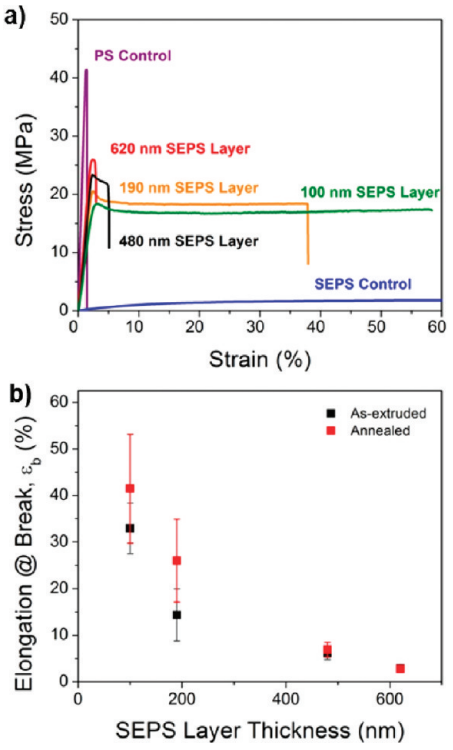

Figure 9. Mechanical response of annealed 257 multilayer films of PS/SEPS. (a) Stress−strain response. (b) Effect of layer thickness on the elongation-at-break.

The mechanical properties of the annealed multilayer films were analyzed to better understand the origin of the observed toughness enhancement: nonequilibrium morphology or decreasing layer thickness. The annealed samples deformed in a more homogeneous manner compared to the as-extruded multilayer films under uniaxial tension. A distinct yield point was observed with the annealing unlike the gradual yielding observed in the as-extruded multilayer films, indicative of a more controlled transfer of stress (Figure 9a). The 480 and 620 nm multilayer films failed via brittle fracture, while the thinner layer films showed similar results to that of the previously discussed as-extruded films. The mechanical responses of the annealed samples were within experimental error of the as-extruded films, which resulted in an increase in elongation-at-break, ε_b, and toughness as the layer thickness decreased to 190 nm. There was an enhancement in the stresses that the multilayer films could withstand, which could be attributed to the highly ordered morphology of the BCP providing a uniform mode of deformation (Figure 9b). The mechanical properties derived from the annealed multilayer films were summarized in Table 2. We have attributed the alignment of PS cylinders within the multilayer film to a decreasing layer thickness effect and are currently

Table 2. Mechanical Properties of Annealed PS/SEPS Films via Uniaxial Tensile Testing

	257 layers; 50/50 (v/v)				
	620 nm	480 nm	190 nm	100 nm	SEPS control
elastic modulus (MPa)	1557 ± 562	1183 ± 105	1085 ± 152	745 ± 270	1.23 ± 0.015
elongation-at-break ε_b (%)	2.77 ± 0.50	6.93 ± 1.58	26.02 ± 19.13	41.46 ± 16.18	510.77 ± 13.64
ultimate tensile strength (MPa)	23.42 ± 2.57	24.40 ± 1.80	21.52 ± 2.31	19.30 ± 1.21	6.59 ± 1.44
toughness (MJ/m^3)	0.41 ± 0.11	1.30 ± 0.30	2.41 ± 2.90	7.17 ± 2.46	16.85 ± 3.75

investigating the deformation mechanics of SEPS under confinement.

CONCLUSIONS

In this research, an elastomeric BCP was confined via the coextrusion multilayer process, resulting in a polymeric multilayer composite with enhanced mechanical toughness. Toughening was attributed to a layer thickness effect, in which the mode of deformation changed from crazing to shear banding as the SEPS layer decreases to ~200 nm. The microlayering process aligned the PS cylinders of the BCP in the extrusion direction, which led to anisotropic scattering patterns from the distortion of the equilibrium array of the microdomains. Upon annealing of the multilayer films, the mechanical integrity was maintained, confirming that there was a layer-thickness-dependent toughening mechanism that led to a shift mode of deformation. The morphology of the BCP when annealed became highly oriented and revealed long-range ordering upon confinement, resulting in hexagonal close packing when the layer thickness decreased to ~200 nm. Further investigation will focus on connecting BCP morphology with layer thicknesses in multilayer films to understand the microdeformation mechanics.

ASSOCIATED CONTENT

Supporting Information. Melt flow indices (MFI), differential scanning calorimetry (DSC), dynamic mechanical analysis (DMA) plots, and small-angle X-ray scattering (SAXS). This material is available free of charge via the Internet at http://pubs.acs.org.

AUTHOR INFORMATION

Corresponding Author
*Phone: (216) 368-1421. E-mail: lashanda.korley@case.edu.

ACKNOWLEDGMENT

This research was supported by the NSF Science and Technology Center through the Center for Layered Polymeric Systems, CLiPS under Grant 0423914. A portion of these studies were conducted at the Swagelock Center for Surface Analysis of Materials (SCSAM) at Case Western Reserve University (confocal microscopy; transmission electron microscopy). Use of the National Synchrotron Light Source (X27C), Brookhaven National Laboratory, was supported by the U.S. Department of Energy, Office of Science, Office of Basic Energy Sciences, under Contract No. DE-AC02-98CH10886. The authors would also like to Alex Jordan, Dr. David Stone, Professor Chris Ellison at University of Texas, Austin, and Chuanyar Lai for their helpful comments as well as Nandula Wanasekara and Seyedali Monemian for assistance with AFM and TEM, respectively.

REFERENCES

(1) Hamley, I. *The Physics of Block Copolymers*; Oxford Science Publications: Oxford, U.K., 1998.
(2) Bates, F. S.; Fredrickson, G. H. *Annu. Rev. Phys. Chem.* **1990**, *41*, 525–557.
(3) Fredrickson, G. H.; Bates, F. S. *Annu. Rev. Mater. Sci.* **1996**, *26*, 501–550.
(4) Matsen, M. W.; Bates, F. S. *Macromolecules* **1996**, *29*, 7641–7644.
(5) Matsen, M. W.; Bates, F. S. *Macromolecules* **1996**, *29*, 1091–1098.
(6) Sakurai, S. *Trends Polym. Sci.* **1997**, *5*, 210–212.
(7) Sakurai, S.; Hashimoto, T.; Fetters, L. J. *Macromolecules* **1995**, *28*, 7947–7949.
(8) Mundra, M. K.; Ellison, C. J.; Behling, R. E.; Torkelson, J. M. *Polymer* **2006**, *47*, 7747–7759.
(9) Koneripalli, N.; Levicky, R.; Bates, F. S.; Ankner, J.; Kaiser, H.; Satija, S. K. *Langmuir* **1996**, *12*, 6681–6690.
(10) Frank, B.; Gast, A. P.; Russell, T. P.; Brown, H. R.; Hawker, C. J. *Macromolecules* **1996**, *29*, 6531–6534.
(11) Koneripalli, N.; Singh, N.; Levicky, R.; Bates, F. S.; Gallagher, P. D.; Satija, S. K. *Macromolecules* **1995**, *28*, 2897–2904.
(12) Nick, L.; Lippitz, A.; Unger, W.; Kindermann, A.; Fuhrmann, J. *Langmuir* **1995**, *11*, 1912–1916.
(13) Angerman, H. J.; Johner, A.; Semenov, A. N. *Macromolecules* **2006**, *39*, 6210–6220.
(14) Huang, Y. M.; Liu, H. L.; Hu, Y. *Macromol. Theory Simul.* **2006**, *15*, 117–127.
(15) Knoll, A.; Horvat, A.; Lyakhova, K. S.; Krausch, G.; Sevink, G. J. A.; Zvelindovsky, A. V.; Magerle, R. *Phys. Rev. Lett.* **2002**, *89*, 035501.
(16) Knoll, A.; Magerle, R.; Krausch, G. *J. Chem. Phys.* **2004**, *120*, 1105–1116.
(17) Zettl, U.; Knoll, A.; Tsarkova, L. *Langmuir* **2010**, *26*, 6610–6617.
(18) Horvat, A.; Lyakhova, K.; Sevink, G.; Zvelindovsky, A.; Magerle, R. *J. Chem. Phys.* **2004**, 1117–1126.
(19) Kim, G.; Libera, M. *Macromolecules* **1998**, *31*, 2569–2577.
(20) Park, I.; Lee, B.; Ryu, J.; Im, K.; Yoon, J.; Ree, M.; Chang, T. *Macromolecules* **2005**, *38*, 10532–10536.
(21) Matsen, M. W. *J. Chem. Phys.* **1997**, *106*, 7781–7791.
(22) Yu, B.; Jin, Q. H.; Ding, D. T.; Li, B. H.; Shi, A. C. *Macromolecules* **2008**, *41*, 4042–4054.
(23) Xiang, H. Q.; Shin, K.; Kim, T.; Moon, S. I.; McCarthy, T. J.; Russell, T. P. *Macromolecules* **2004**, *37*, 5660–5664.
(24) Kamperman, M.; Korley, L.; Yau, B.; Johansen, K.; Joo, Y.; Wiesner, U. *Polym. Chem.* **2010**, 1001–1004.
(25) Pethe, V. V.; Wang, H. P.; Hiltner, A.; Baer, E.; Freeman, B. D. *J. Appl. Polym. Sci.* **2008**, *110*, 1411–1419.
(26) Ranade, A. P.; Hiltner, A.; Baer, E.; Bland, D. G. *J. Cell. Plast.* **2004**, *40*, 497–507.
(27) Baer, E.; Hiltner, A.; Jarus, D. *Macromol. Symp.* **1999**, *147*, 37–61.
(28) Kazmierczak, T.; Song, H. M.; Hiltner, A.; Baer, E. *Macromol. Rapid Commun.* **2007**, *28*, 2210–2216.
(29) Tangirala, R.; Baer, E.; Hiltner, A.; Weder, C. *Adv. Funct. Mater.* **2004**, *14*, 595–604.
(30) Ma, M.; Vijayan, K.; Hiltner, A.; Baer, E.; Im, J. *J. Mater. Sci.* **1990**, *25*, 2039–2046.
(31) Mueller, C.; Nazarenko, S.; Ebeling, T.; Schuman, T.; Hiltner, A.; Baer, E. *Polym. Eng. Sci.* **1997**, 355–362.
(32) Mueller, C. D.; Kerns, J.; Ebeling, T.; Nazarenko, S.; Hiltner, A.; Baer, E. In *Polymer Process Engineering 97*; Coates, P. D., Ed.; The Institute of Materials: London, 1997; pp 137−157.
(33) Liu, R. Y. F.; Jin, Y.; Hiltner, A.; Baer, E. *Macromol. Rapid Commun.* **2003**, *24*, 943–948.
(34) Liu, R. Y. F.; Bernal-Lara, T. E.; Hiltner, A.; Baer, E. *Macromolecules* **2004**, *37*, 6972–6979.
(35) Liu, R. Y. F.; Ranade, A. P.; Wang, H. P.; Bernal-Lara, T. E.; Hiltner, A.; Baer, E. *Macromolecules* **2005**, *38*, 10721–10727.
(36) Kerns, J.; Hsieh, A.; Hiltner, A.; Baer, E. *J. Appl. Polym. Sci.* **2000**, *77*, 1545–1557.
(37) Sung, K.; Hiltner, A.; Baer, E. *J. Mater. Sci.* **1994**, *29*, 5559–5568.
(38) Sung, K.; Haderski, D.; Hiltner, A.; Baer, E. *J. Appl. Polym. Sci.* **1994**, *52*, 147–162.
(39) Michler, G. H.; Adhikari, R.; Lebek, W.; Goerlitz, S.; Weidisch, R.; Knoll, K. *J. Appl. Polym. Sci.* **2002**, *85*, 683–700.

(40) *ASTM Standard D638 2010: Standard Test Method for Tensile Properties of Plastics*; ASTM International: West Conshohocken, PA, 2010; 10.1520/D0638−10; www.astm.org.
(41) Michler, G. H. *Mechanical Properties of Polymers Based on Nanostructure and Morphology*, 1st ed.; CRC Press: Boca Raton, FL, 2005; pp 419−426.
(42) Ponting, M.; Burt, T. M.; Korley, L. T. J.; Andrews, J.; Hiltner, A.; Baer, E. *Ind. Eng. Chem. Res.* **2010**, *49*, 12111–12118.
(43) Sakurai, S.; Momii, T.; Taie, K.; Shibayama, M.; Nomura, S.; Hashimoto, T. *Macromolecules* **1993**, *26*, 485–491.
(44) Keller, A.; Pedemonte, E.; Willmouth, F. M. *Nature* **1970**, *225*, 538–539.
(45) Park, S. M.; Stoykovich, M. P.; Ruiz, R.; Zhang, Y.; Black, C.; T; Nealey, P.; F *Adv. Mater.* **2007**, *19*, 607–611.